COMPONENT PART NOTICE

THIS PAPER IS A COMPONENT PART OF THE FOLLOWING COMPILATION REPORT:

(TITLE): The Effect of the Ionosphere on Radiowave Signals and Systems Performance Based on Ionospheric Effects Symposium Held on 1-3 May 1990.

(SOURCE): Naval Research Lab., Washington, DC

TO ORDER THE COMPLETE COMPILATION REPORT USE AD-A233 797.

THE COMPONENT PART IS PROVIDED HERE TO ALLOW USERS ACCESS TO INDIVIDUALLY AUTHORED SECTIONS OF PROCEEDINGS, ANNALS, SYMPOSIA, ETC. HOWEVER, THE COMPONENT SHOULD BE CONSIDERED WITHIN THE CONTEXT OF THE OVERALL COMPILATION REPORT AND NOT AS A STAND-ALONE TECHNICAL REPORT.

THE FOLLOWING COMPONENT PART NUMBERS COMPRISE THE COMPILATION REPORT:

AD#:	TITLE:
AD-P006 265 thru AD-P006 325	

Accesion For	
NTIS CRA&I	☑
DTIC TAB	☐
Unannounced	☐
Justification	
By	
Distribution /	
Availability Codes	
Dist	Avail and / or Special
A-1	

VHF/UHF RADAR SCINTILLATION EFFECTS OBSERVED BY ALTAIR

Dennis L. Knepp and Harry L. F. Houpis
Mission Research Corporation
Carmel, California

ABSTRACT

During the Defense Nuclear Agency (DNA) PEAK (Propagation Effects Assessment - Kwajalein) experiment in August 1988, the ALTAIR VHF/UHF wide bandwidth radar was used to track spherical satellites in low-earth orbit. The purpose of the experiment was to obtain radar data during the most severe propagation disturbances available naturally. The PEAK experiment has been quite successful, giving many measurements of strong scintillation as well as the first measurements of frequency-selective fading on propagating radar pulses. This high level of scintillation severity is statistically similar to that likely to be encountered over large spatial and temporal extent if the ionosphere were disturbed by a high-altitude nuclear detonation.

This paper describes the measurements that were obtained during the track of several spherical U.S. and Soviet calibration satellites. The use of spherical satellites eliminates the problem of target glint that causes fluctuation in the received signal due to interference from multiple target scatterers. Unique measurements were obtained during PEAK of severe frequency-selective scintillation during several passes of Cosmos 1427, a 2-meter diameter sphere.

In this paper the experimental results are used to demonstrate an enhancement in the average received power that is observed during severe scintillation. The observed statistics of the enhancement are compared to analytic calculations using the Nakagami-m distribution with very good agreement. This previously unreported enhancement is predictable on the basis of the first-order amplitude statistics for two-way radar propagation in a monostatic propagation geometry as well as by a more thorough analysis using reciprocity; both analytic approaches are presented here. The enhancement is important for both ground and space-based radars that have to operate during scintillation, since as much as a 3 decibel increase in the target (and clutter) signal-to-noise ratio is possible, depending on the severity of the scintillation and on the radar transmit/receive geometry.

INTRODUCTION

It is well-known that a propagating signal in the frequency range from VHF to L-band can experience disturbances due to naturally occurring F-region ionization. Disturbances due to mean or average ionization consisting of dispersion, refraction, Faraday rotation, and phase shift have been the subject of research work over the last several decades and are well understood [*Lawrence, et al.*, 1964]. Disturbances due to smaller scale electron-density irregularities that produce scintillation of propagating waves are the subject of current research [*Basu, et al.*, 1987].

Scintillation consists of the rapid variation of signal phase, amplitude, angle-of-arrival, time-of-arrival and other signal properties. Intense signal scintillation is often observed over satellite links and in radar measurements [*Towle*, 1980] through the ambient ionosphere at VHF and UHF. Strong equatorial scintillation is even observed at frequencies as high as C-band, but rarely [*Franke, et al.*, 1984]. The regions of scintillation consist of a 20° wide belt of latitude centered around the geomagnetic equator and the polar regions above 55° – 60° latitude. Within the equatorial scintillation belt, Rayleigh scintillation is often experienced at frequencies in the VHF to UHF range during the late evening and early morning hours from about 2000-0200 local time.

The DNA PEAK experiment was developed with the major goal of using the severely disturbed ionospheric

propagation channel to measure and record worst-case propagation effects. The primary experiment utilized ALTAIR, a high-performance long range VHF/UHF tracking radar. The ALTAIR VHF signal is of prime interest since the lower frequency experiences the greatest degree of scintillation. The goal of the DNA program is to measure radar signal propagation effects, determine the irregularity structure, measure the radar performance degradation, and then to relate the performance degradation to the measured propagation disturbances and to the *in-situ* irregularity structure. Once these relationships are established and verified from the experimental data, work can be directed towards the development of mitigation techniques to improve radar performance during signal disturbances.

ALTAIR WAVEFORM DESCRIPTION

ALTAIR utilizes a circular antenna with a diameter of 150 feet. The 3 dB beamwidths are 2.8 degrees at VHF and 1.1 degrees at UHF. In the PEAK experiment, independent range tracks were maintained at both frequencies, but the UHF angle information was used to steer the antenna. For the satellite tracking portion of the DNA PEAK experiment, the VHF and UHF waveforms chosen corresponded to the maximum bandwidth available. This selection gives an LFM waveform with a chirping bandwidth of 7.1 MHz at VHF and 18 MHz at UHF but limits the maximum pulse repetition frequency to 372 Hz. The actual PRF is determined by the radar control system to avoid eclipsing of pulses (i.e., to avoid reception of a pulse when the radar is transmitting).

The VHF range sample (or range gate) spacing is 30 meters, corresponding to a temporal sampling interval of 20 μsec. However, the minimum Nyquist rate for a 7 MHz chirp corresponds to a maximum sampling interval of about 14 μsec. Thus the recorded dechirped pulses are somewhat undersampled, which limits our measurements of pulse distortion. At UHF the pulses are undersampled by a greater proportion (15 m spacing), but since no pulse distortion due to scattering was observed this is of no concern.

The following signal parameters have been found to be important in the determination of the effects of fading on radar and communications system performance.

Scintillation Index (S_4). The level of amplitude scintillation is often measured by the S_4 scintillation index defined as the normalized standard deviation of the RCS obtained from a constant-RCS target.

$$S_4^2 = \frac{\langle P^2 \rangle - \langle P \rangle^2}{\langle P \rangle^2} \tag{1}$$

where P is the apparent radar RCS (the fluctuations in P are due to scintillation) and the angle brackets denote a stochastic average. Values of S_4 on a one-way path generally range from a minimum of zero signifying no scintillation to a maximum of unity indicating worst-case Rayleigh fading where the quadrature components of the received (one-way) signal are uncorrelated Gaussian variates.

With the ALTAIR data collected during PEAK it is possible to measure the signal-to-noise ratio (SNR) and correct the measured S_4 for noise effects using the expression

$$S_4^2(\text{scint}) = S_4^2(\text{measured}) \left(1 + \frac{1}{SNR}\right)^2 - \frac{2}{SNR} - \frac{1}{SNR^2} \tag{2}$$

This expression is obtained by calculating the value of S_4 due to a random desired signal in the presence of white Gaussian noise. To measure a value of S_4, 1000 or 1500 values of sampled RCS measurements (corresponding to about 3 seconds of data during the satellite pass) were averaged.

Signal Decorrelation Time (τ_0). The signal decorrelation time, τ_0 is an appropriate quantity to describe the fading rate (the fading rate is $1/\tau_0$) of the received signal. The quantity τ_0 is defined by the expression

$$\langle E(t+\tau)E^*(t) \rangle = |E_0|^2 \exp\{-\tau^2/\tau_0^2\} \tag{3}$$

which is the correlation function of the complex received signal voltage. The actual value of τ_0 is a function of radar geometry and of the irregularity structure and intensity of the disturbed ionospheric channel. Large values of τ_0 correspond to slow fading conditions and small values correspond to fast fading. Both types of fading can degrade radar performance.

To measure τ_0 from the recorded I and Q quadrature data, the signal phase variations due to target motion must first be removed. That is, range variations and temporal variation in the gross total electron content (TEC) encountered as the line-of-sight traverses the ionosphere give deterministic phase variations not associated with scintillation.

Fortunately, simultaneous ALTAIR VHF and UHF pulses are designed for accurate TEC measurement through the use of range measurements at two frequencies. Once geometric range and TEC are measured pulse-by-pulse, they are smoothed in 10-second segments through polynomial fitting, and the phase changes due to range and TEC are separately removed from the recorded quadrature data. The resulting fluctuations in the complex received signal are due only to propagation effects, and τ_0 is easily measured through the use of FFT techniques. To obtain τ_0, the value of time lag corresponding to the $1/e$ point of the magnitude of the autocorrelation function is utilized.

Channel Coherence Bandwidth (f_0). The channel coherence bandwidth is a measure of the maximum bandwidth available in the propagation channel over which it is possible to transmit a signal without undesired pulse distortion. If the signal spectral components are separated in frequency by an amount greater than the coherence bandwidth, different spectral components will undergo uncorrelated fading. This distortion in the received signal spectrum causes the received time domain signal to display undesired time sidelobes. The terminology "frequency-selective fading" is synonymous with the increased importance of multipath wherein the signal propagates over many transmission paths, interfering coherently with less-timely versions of itself. The value of f_0 is quite important to many aspects of radar design.

The equation for the rms time-delay spread is the defining expression for f_0

$$\sigma_\tau^2 = \frac{\sum P(\tau_i)\tau_i^2}{\sum P(\tau_i)} - \langle\tau\rangle^2, \text{ where } \langle\tau\rangle = \sum P(\tau_i)\tau_i / \sum P(\tau_i) \tag{4}$$

In this equation $P(\tau_i)$ is the sampled received signal power at the output of the matched filter. Now the received signal can be written as the convolution of three components, that due to the dechirped signal itself (with no ionospheric effects); a second component due to the dispersive spreading caused by mean ionization along the propagation path; and a third component due to the frequency-selective scintillation. It is easy to show that

$$\sigma_\tau^2 = \sigma_{\text{pulse}}^2 + \sigma_{\text{tec}}^2 + \sigma_{\text{scint}}^2 \tag{5}$$

The quantity f_0 is defined as $1/2\pi\sigma_{\text{scint}}$; it represents only that portion of the signal spread due to scintillation or multipath.

During the PEAK experiment, $P(\tau_i)$ was recorded at VHF using range-gate samples separated by 30 meters, corresponding to a temporal spacing of 20μ sec. As discussed above, this temporal spacing is greater than the Nyquist interval; consequently measurements of moments of the pulse must be treated with caution.

In our measurements of the pulse spread, the recorded pulse shapes were collected into groups of 100, then the average pulse shape was obtained by noncoherent summation. The moments of this average pulse were obtained using Equation 4. We have not yet removed the σ_{tec}^2 term, so our current measurements of f_0 include the effects of dispersion.

ALTAIR MULTIPATH DATA

Figures 1-2 show a sequence of plots of the recorded received VHF pulse shapes (power versus range) from Cosmos 1427. Cosmos 1427 is a 2-meter diameter calibration sphere in a near polar orbit at an altitude of about 420 km. Figure 1, taken from satellite pass PEAK 4H, is an example of 50 sequential pulses recorded during a near-overhead pass with resultant high SNR (about 35 dB) during the period shown. Each pulse shape shows received power (plotted in dB above a milliwatt) versus range-gate sample. The first pulse at ALTAIR TAG time (time measured from the start of track) of 670.03 seconds is plotted at the bottom of the figure; subsequent pulses are offset above and to the right of the first.

Figure 2 gives an example of the most severely disturbed radar pulse data recorded during ionospheric fading conditions. This example shows 50 sequential pulses recorded using Cosmos 1427 during PEAK 9C over a period of about 140 msec starting at ALTAIR TAG time 157.2 msec. The temporal effect of fading is evident in the rather smooth variation of the peak power with time. The severe effects of ionospheric multipath are evident through the appearance of multiple peaks in the individual pulse shapes. Such pulse distortion will degrade many aspects of radar performance including detection, tracking, imaging, etc.

Figure 3 gives measurements of S_4, τ_0, and f_0 at VHF as a function of time during PEAK 9C. It is seen that saturated scintillation (S_4 (two-way)=$\sqrt{5}$) is experienced for much of the time duration between 135 and 220 seconds. Minimum values of τ_0 are around 10 msec; minimum values of f_0 are around 0.5 MHz.

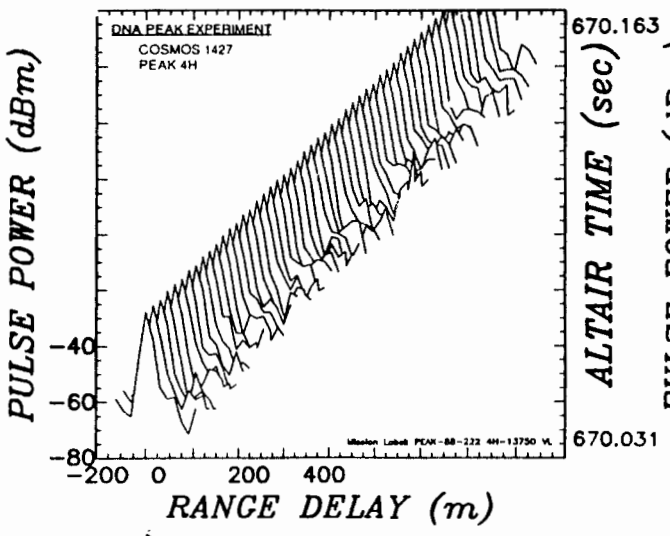

Figure 1. ALTAIR VHF pulse shapes during undisturbed conditions.

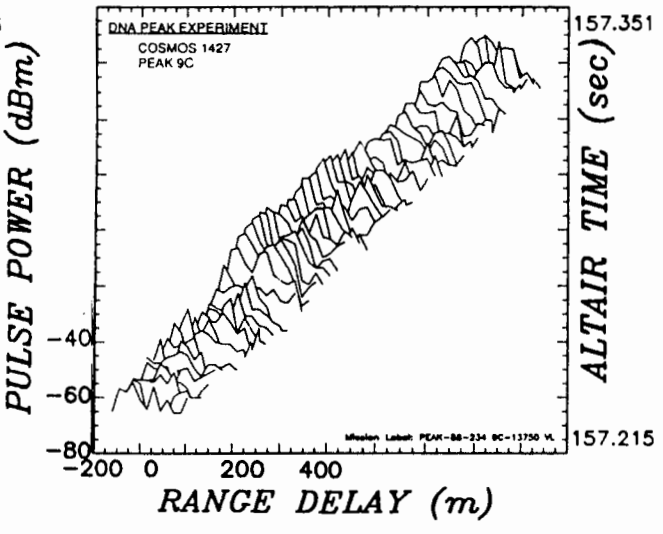

Figure 2. ALTAIR VHF pulse shapes during severe multipath.

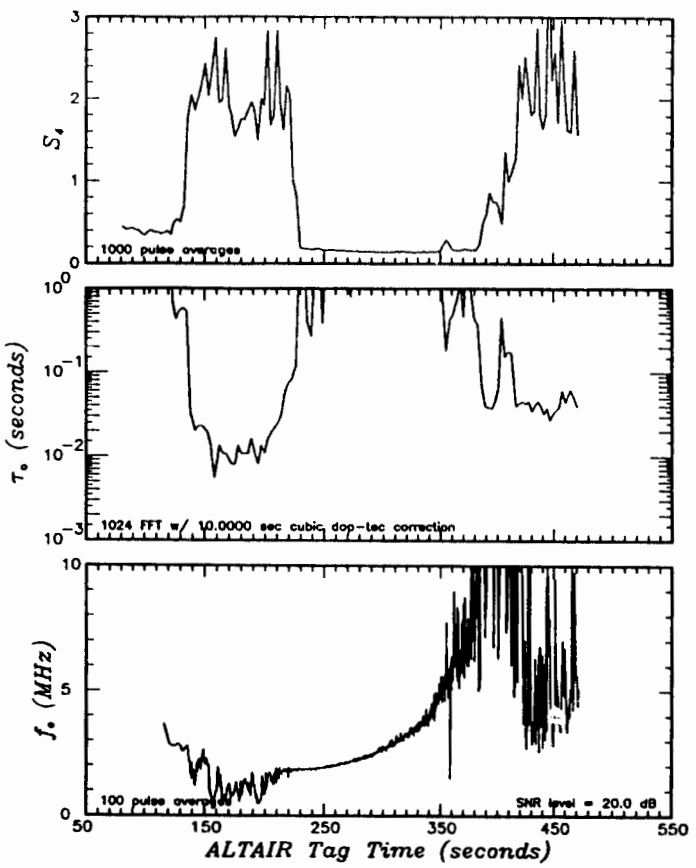

Figure 3. Statistical signal parameters measured during severe scintillation.

Note that the measurements of S_4 exceed in several cases the maximum value $\sqrt{5} = 2.24$, valid for saturated scintillation. This is the result of focusing caused by large scale irregularities "close to" the radar location. Equivalently, the Fresnel zone size is larger than the freezing scales of the irregularities.

THEORY OF POWER ENHANCEMENT

In the following a simple expression is obtained for the two-frequency, two-position, two-time mutual coherence function (MCF) for the case of two-way propagation from a radar antenna to a point target and back to the antenna. The result is given in terms of products of the one-way MCFs for propagation from the radar target to the radar transmit and receive locations and is valid for saturated scintillation where the quadrature components of the signal, after one-way propagation, are uncorrelated Gaussian variates. This result explains the enhancement as caused by correlation of the wave that propagates from the radar location to the target with the wave that propagates from the target to the radar.

Consider the problem illustrated in Figure 4 of a wave transmitted at time t at a center radian frequency of ω with time dependence $\exp(i\omega t)$ from an aperture antenna located in the ρ_x-plane at $\bar{\rho}_T$. *Fante* [1985], gives the received field using the Huygens-Fresnel Principle under two important assumptions. First, the transmitted signal must be narrow-band about the center radian frequency ω, and second, the time rate of change of the index-of-refraction fluctuations and of the transmitted temporal envelope must be slow in comparison to the radian frequency ω. These conditions are generally satisfied in modern pulsed radars. In this case the field received after propagation from the antenna to a location in the plane of the scattering layer, $\bar{\rho}_\xi$ is

$$E_{\text{inc}}\left(\bar{\rho}_\xi, \omega, t + \frac{Z_t}{c}\right) = \int d\rho_x^2 A(\bar{\rho}_x - \bar{\rho}_T) G_1(\bar{\rho}_x \rightarrow \bar{\rho}_\xi; \omega; t) E_0(\bar{\rho}_x, \omega) \tag{6}$$

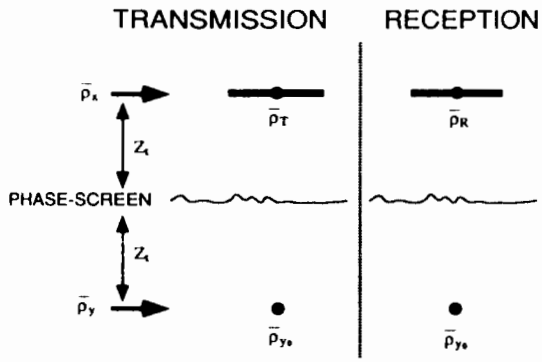

Figure 4. Two-way scattering geometry.

From the figure Z_t is the distance along the direction of propagation from the transmitter plane to a scattering layer represented here as a thin phase-screen, although the thin phase-screen assumption is not required. The quantity Z_r is the distance from the scattering layer to the target location, $E_0(\bar{\rho}_x, \omega)$ is the frequency-domain representation of the signal transmitted from location $\bar{\rho}_x$ and $A(\bar{\rho}_x - \bar{\rho}_T)$ is the aperture weighting function for the transmit antenna located at position $\bar{\rho}_T$. For example, the choice $A(\bar{\rho})$ = constant for $|\bar{\rho}| \leq \rho_0$ and zero otherwise is appropriate for a circular antenna. The time dependence t in the propagator G_1, given by Equation 7, signifies that the transmission occurs at time t. The signal arrives at the scattering layer at a later time, $t + Z_t/c$ as included in the expression for E_{inc}. The propagator is given as

$$G_1(\bar{\rho}_x \rightarrow \bar{\rho}_\xi; \omega; t) = \frac{k}{i2\pi Z_t} \exp\left\{-ikZ_t - \frac{ik}{2Z_t}(\bar{\rho}_\xi - \bar{\rho}_x)^2\right\} \tag{7}$$

Now the signal in the target plane may be written by propagating in the same manner from the scattering layer down to the target. The result can be expressed as

$$E_{\text{tar}}(\bar{\rho}_y, \omega, t + \tau) = \int d\rho_\xi^2 E_{\text{inc}}\left(\bar{\rho}_\xi, \omega, t + \frac{Z_t}{c}\right) G_2\left(\bar{\rho}_\xi \rightarrow \bar{\rho}_y; \omega; t + \frac{Z_t}{c}\right) \tag{8}$$

where the propagator, G_2 accounts for propagation of a wave starting from the layer at time $t + Z_t/c$, and includes the phase term ϕ which gives the scattering layer contribution to the phase in the Huygens-Fresnel principle.

$$G_2\left(\bar{\rho}_\xi \to \bar{\rho}_y;\omega;t+\frac{Z_t}{c}\right)=\frac{k}{i2\pi Z_r}\exp\left\{-ikZ_r-\frac{ik}{2Z_r}(\bar{\rho}_\xi-\bar{\rho}_y)^2\right\}\exp\left\{i\phi\left(\bar{\rho}_\xi,\omega,t+\frac{Z_t}{c}\right)\right\} \tag{9}$$

For simplification, the above three equations can be combined as

$$E_{\text{tar}}(\bar{\rho}_y,\omega,t+\tau)=\int d\rho_x^2 A(\bar{\rho}_x-\bar{\rho}_T)G_{\text{down}}(\bar{\rho}_x\to\bar{\rho}_y;\omega;t)E_0(\bar{\rho}_x,\omega) \tag{10}$$

which represents downward propagation of a wave from the ρ_x-plane starting at time t, to the ρ_y-plane or target plane, arriving at time $t+\tau$ where $\tau=(Z_t+Z_r)/c$. The quantity G_{down} is a time-variable (varying with t) transfer function for a sinusoid of radian frequency ω.

Now let the target be a point scatterer with unity reflectivity and located at $\bar{\rho}_{y_0}$. Then the field received at time $t+2\tau$ after upward propagation from the target back to the radar location is given as

$$E_{\text{rcv}}(\bar{\rho}_R,\omega,t+2\tau)=\int d\rho_x^2 B(\bar{\rho}_x-\bar{\rho}_R)G_{\text{up}}(\bar{\rho}_{y_0}\to\bar{\rho}_x;\omega;t+\tau)E_{\text{tar}}(\bar{\rho}_{y_0},\omega,t+\tau) \tag{11}$$

Equations 10-11 can be combined to yield a simplified expression

$$\begin{aligned}E_{\text{rcv}}(\bar{\rho}_R,\omega,t+2\tau) &= \int d\rho_x'^2 d\rho_x''^2 A(\bar{\rho}_x'-\bar{\rho}_T)B(\bar{\rho}_x''-\bar{\rho}_R)\\ &\quad G_{\text{up}}(\bar{\rho}_{y_0}\to\bar{\rho}_x'';\omega;t+\tau)G_{\text{down}}(\bar{\rho}_x'\to\bar{\rho}_{y_0};\omega;t)\;E_0(\bar{\rho}_x',\omega)\end{aligned} \tag{12}$$

where the quantity $B(\bar{\rho}_x''-\bar{\rho}_R)$ specifies the aperture weighting function for the receive antenna which is located with its phase-center at $\bar{\rho}_R$ at time $t+2\tau$. Now simplify by letting both transmit and receive apertures be point antennas so $A(\bar{\rho}_x'-\bar{\rho}_T)=\delta(\bar{\rho}_x'-\bar{\rho}_T)$ and similarly for B so that the expression above for the received field after two-way propagation contains no explicit integrals. Then the expression for the desired autocorrelation function after two-way propagation is obtained as

$$\begin{aligned}\Gamma_2(\bar{\rho}_{R1}-\bar{\rho}_{R2};\omega_1-\omega_2;\Delta) &= \langle E_{\text{rcv}}(\bar{\rho}_{R1},\omega_1,t+2\tau+\Delta)E_{\text{rcv}}^*(\bar{\rho}_{R2},\omega_2,t+2\tau)\rangle\\ &= \langle G_{\text{up}}(\bar{\rho}_{y_0}\to\bar{\rho}_{R1};\omega_1;t+\tau+\Delta)G_{\text{down}}(\bar{\rho}_{T1}\to\bar{\rho}_{y_0};\omega_1;t+\Delta)\\ &\quad G_{\text{up}}^*(\bar{\rho}_{y_0}\to\bar{\rho}_{R2};\omega_2;t+\tau)G_{\text{down}}^*(\bar{\rho}_{T2}\to\bar{\rho}_{y_0};\omega_2;t))\;E_0(\bar{\rho}_{T1},\omega_1)E_0^*(\bar{\rho}_{T2},\omega_2)\end{aligned} \tag{13}$$

where the angle brackets denote stochastic average. $E_{\text{rcv}}(\bar{\rho}_{R1})$ is the voltage received at $\bar{\rho}_{R1}$, due to a transmitter at $\bar{\rho}_{T1}$; $E_{\text{rcv}}(\bar{\rho}_{R2})$ is the voltage received at $\bar{\rho}_{R2}$ due to a transmitter at $\bar{\rho}_{T2}$. To proceed further, reciprocity must be invoked to relate upward and down-going waves through the expression

$$G_{\text{down}}(\bar{\rho}_x\to\bar{\rho}_y;\omega;t)=G_{\text{up}}\left(\bar{\rho}_y\to\bar{\rho}_x;\omega;t+\frac{Z_t-Z_r}{c}\right) \tag{14}$$

The above equation states reciprocity as follows. In propagating downward, starting at time t, the wave arrives at the layer at time $t+Z_t/c$; in upward propagation starting at time $t+(Z_t-Z_r)/c$, the wave arrives at the screen at time $t+(Z_t-Z_r)/c+Z_r/c=t+Z_t/c$, i.e., the same time. Thus the scattering layer is in the same position for upward as it is for downward propagation, so reciprocity holds.

Application of reciprocity allows one to replace the downward-going transfer functions in Equation 13 with their equivalent upward-going transfer functions.

$$\begin{aligned}\Gamma_2 &= \left\langle G_{\text{up}}(\bar{\rho}_{y_0}\to\bar{\rho}_{R1};\omega_1;t+\tau+\Delta)G_{\text{up}}\left(\bar{\rho}_{y_0}\to\bar{\rho}_{T1};\omega_1;t+\Delta+\frac{Z_t-Z_r}{c}\right)\right.\\ &\quad \left. G_{\text{up}}^*(\bar{\rho}_{y_0}\to\bar{\rho}_{R2};\omega_2;t+\tau)G_{\text{up}}^*\left(\bar{\rho}_{y_0}\to\bar{\rho}_{T2};\omega_2;t+\frac{Z_t-Z_r}{c}\right)\right\rangle\; E_0(\bar{\rho}_{T1},\omega_1)E_0^*(\bar{\rho}_{T2},\omega_2)\end{aligned} \tag{15}$$

Now, if scintillation is saturated on a one-way propagation path so that G_{up} is a complex Gaussian variate, then one can write the fourth-order moment using the well-known expression $\langle x_1x_2x_3x_4\rangle=\langle x_1x_2\rangle\langle x_3x_4\rangle+\langle x_1x_3\rangle\langle x_2x_4\rangle+\langle x_1x_4\rangle\langle x_2x_3\rangle$.

In the application of this expression for the fourth-order moments, the term $\langle G_{\text{up}}G_{\text{up}}\rangle\langle G_{\text{up}}^*G_{\text{up}}^*\rangle$ is found to be of the form $(\langle Re^2\rangle-\langle Im^2\rangle)^2$ where the variances of real and imaginary parts are equal, giving zero. The other two terms are written in Equation 16 as the products of MCFs valid for the upward path (Γ_{up}) from the target to the various transmitter and receiver locations. Γ_{20} is the two-way MCF in the absence of a scattering layer.

$$\begin{aligned}\Gamma_2 &= \Gamma_{20}\{\Gamma_{up}(\bar{\rho}_{R1}-\bar{\rho}_{R2};\omega_1-\omega_2;\Delta)\Gamma_{up}(\bar{\rho}_{T1}-\bar{\rho}_{T2};\omega_1-\omega_2;\Delta)\\ &+ \Gamma_{up}\left(\bar{\rho}_{R1}-\bar{\rho}_{T2};\omega_1-\omega_2;\Delta-\frac{2Z_r}{c}\right)\Gamma_{up}\left(\bar{\rho}_{T1}-\bar{\rho}_{R2};\omega_1-\omega_2;\Delta+\frac{2Z_r}{c}\right)\}\\ &\bar{E}_0(\bar{\rho}_{T1},\omega_1)E_0^*(\bar{\rho}_{T2},\omega_2)\end{aligned} \tag{16}$$

The quantity $\bar{\rho}_{T1}$ is the transmitter location at time $t+\Delta$; $\bar{\rho}_{T2}$ is the transmitter location at time t; $\bar{\rho}_{R1}$ and $\bar{\rho}_{R2}$ are the receiver locations at times $t+2\tau+\Delta$ and $t+2\tau$, respectively.

The quantity $2Z_r/c$ is the time required for the wave to propagate from the scattering layer, to the target, and back to the scattering layer. This quantity then represents the temporal interval of importance to the correlation of down-going and up-going waves.

Expressions for Γ_{up} and Γ_{20} for this geometry are given in *Knepp* [1983; 1985] as

$$\Gamma_{up}(\bar{\rho},\omega_d,t) = (1+i\omega_d/\omega_{coh})^{-1}\exp\left\{-\sigma_\phi^2\omega_d^2/2\omega_0^2\right\}\exp\left\{\frac{-\rho^2/\ell_0^2}{1+i\omega_d/\omega_{coh}}\right\}\exp\left\{-t^2/\tau_c^2\right\} \tag{17}$$

$$\Gamma_{20} = \left(\frac{1}{Z_r+Z_t}\right)^4\exp\left\{\frac{-ik_1(\rho_{R1}^2+\rho_{T1}^2)+ik_2(\rho_{R2}^2+\rho_{T2}^2)}{2(Z_r+Z_t)}\right\} \tag{18}$$

where ω_{coh} is the coherence bandwidth, σ_ϕ is the phase-screen standard deviation, ℓ_0 is the signal decorrelation distance, and $\exp\{-t^2/\tau_c^2\}$ has been added to reflect temporal variation in the scattering layer. The quantities k_1 and k_2 are the wavenumbers at ω_1 and ω_2.

If transmitter and receiver are far away from one another, the second term in Equation 16 is zero, since each Γ_{up} is separately zero. If transmitter and receiver are collocated and $2Z_r/c$ is small, the second term is equal to the first term and thereby represents the enhancement. The enhancement depends on the relative positions of transmitter and receiver at two different times. It is therefore important in the evaluation of the performance of space-based radar, particularly displaced phase center array (DPCA) wherein the transmit and receive apertures have complicated relative motion.

For the case of no scattering, the resulting expression for the MCF is $\Gamma_2(\text{no scint}) = \Gamma_{20}E_0(\bar{\rho}_{T1},\omega_1)E_0^*(\bar{\rho}_{T2},\omega_2)$. For the case of a monostatic radar geometry with small values of the quantity $2Z_r/c$, so that $\Gamma_{up}=1$ in all cases in Equation 16, one obtains $\Gamma_2(\text{monostatic radar}) = 2\Gamma_2(\text{no scintillation})$ or a 3 dB increase in average received power above that measured with no scintillation.

Measurements of the Enhancement. Fairly straightforward analysis enables one to check several aspects of this power enhancement theory. At its simplest the enhancement can be derived using reciprocity which states that, if the propagation environment is unchanging, a signal with a single frequency component traverses the same path in traveling from the radar to the target and back. In that case the voltage after two-way propagation is proportional to the square of the one-way voltage. Under the assumption of Nakagami-m statistics for the one-way power, the probability density function (pdf) of received RCS is given by

$$p_1(S)dS = \frac{mS^{m-1}}{\Gamma(m)\langle S\rangle^m}\exp\left\{\frac{-mS}{\langle S\rangle}\right\}dS,\ S\geq 0,\ (\text{one}-\text{way}) \tag{19}$$

If reciprocity holds, the radar measures the two-way RCS, $Q=S^2$ which then has the pdf given by

$$p_2(Q)dQ = \frac{m^mQ^{m/2-1}}{2\Gamma(m)\langle S\rangle^m}\exp\left\{\frac{-m\sqrt{Q}}{\langle S\rangle}\right\}dQ,\ Q\geq 0,\ (\text{two}-\text{way}) \tag{20}$$

From Equation 20 the mean received two-way power can be computed in terms of the square of the one-way power as $\langle Q\rangle = \int_0^\infty p_2(Q)QdQ = \frac{(m+1)}{m}\langle S\rangle^2$. In the case of a constant signal with no fading, S_4 is zero, m is infinity and one obtains $\langle Q(\text{no scint})\rangle = \langle S\rangle^2$ which can be combined with the above expression to yield a relationship between average RCS and m.

$$\frac{\langle\text{RCS}\rangle}{\langle\text{RCS (no scint)}\rangle} = \frac{m+1}{m} \tag{21}$$

ALTAIR VHF Data Analysis. Figure 5 gives an example of ALTAIR UHF data in which the backscatter enhancement is quite evident. This data was obtained from the track of the Soviet sphere, Cosmos 1427, on the evening of August 21, 1988. This particular satellite pass is referred to as PEAK 9C, data from which is shown in Figures 1-2.

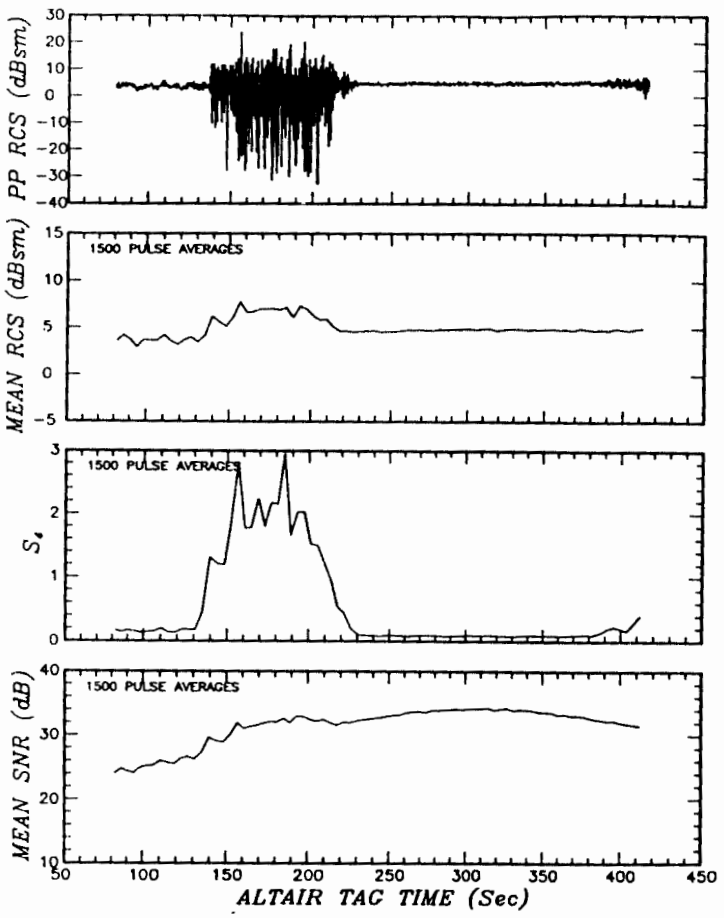

Figure 5. ALTAIR UHF data taken during PEAK 9C.

The top frame of Figure 5 shows the measured UHF radar cross section in decibels below a square meter as a function of time from the start of radar track. In this frame about one-tenth of the recorded data is shown, at a sample spacing of 25 msec. The radar data sampling interval varies but is generally around 2.7 msec. Notice the abrupt onset of a patch of severe scintillation starting at a time of 135 seconds and ending at 220 seconds. The elevation at 140 seconds is 7.5° and is increasing slowly until about 300 seconds when the satellite begins to descend. This high elevation angle rules out ground multipath as the source of the signal fluctuations.

The lower three frames in Figure 5 show computed quantities obtained by averaging the data obtained over 1500 consecutive received pulses. The second frame gives the average RCS. The average is obtained by summing 1500 values of power, dividing the sum by 1500, and then converting to decibels. The third frame gives the values of S_4 computed on each 1500 second segment of data. The bottom frame shows the average signal-to-noise ratio (SNR) computed by averaging the ratio of the power in the track gate to the power in the last recorded range gate. In the case of PEAK 9C, the track gate corresponds to sample number 4, the last recorded sample is number 9. Note that our SNR measurements could be corrupted by range sidelobes, but are not here since the range sidelobes are 35 dB below the peak and, therefore, below the noise, for the most part. Unfortunately, we do not have available for analysis the radar's actual noise power measurement.

The enhancement in received RCS during scintillation is clearly visible in the second frame of Figure 5, which gives the average RCS as a function of TAG time. If one uses the period between 250 to 300 seconds to measure the mean RCS without scintillation, increases in RCS due to scintillation approaching 3 dB are apparent in the period 140-210 seconds.

In Figure 6 the UHF measurements of S_4 and average RCS are combined in a format to check the enhancement theory given above. By using the ALTAIR data shown in Figure 5 it is possible to measure all the values in

Equation 21 to check this relationship. Take the average RCS during undisturbed propagation conditions as the average of the received RCS over the interval 250-300 seconds. Then consider the other measurements of average power and S_4 with (and without) scintillation during the time period 130-380 seconds. These measurements of S_4 are first corrected for noise using Equation 2 and then used to obtain the m-parameter through the expression $S_4^2(\text{two-way}) = (4m^2 + 10m + 6)/(m(m+1)^2)$ [*Knepp and Reinking*, 1989].

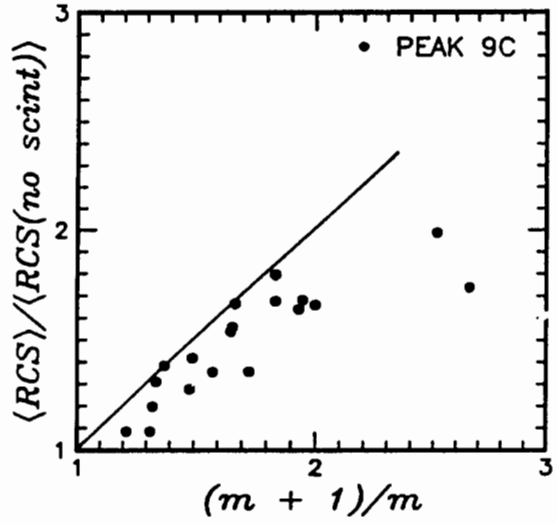

Figure 6. Comparison of ALTAIR measurements to theory, PEAK 9C.

The resulting data is then presented in the form of a scatter plot shown in Figure 6 where the ratio of the average RCS measurements with and without scintillation are plotted as a function of the ratio $(m+1)/m$. A straight line with unity slope corresponds to the enhancement theory described above. The agreement is quite good between measured data and theory for this single pass of Cosmos 1427 near ALTAIR.

Figures 7 and 8 show similar ALTAIR data at UHF and VHF, respectively, for three additional passes of Cosmos 1427 of (PEAK 2G, 7C, 6F) and a pass of a smaller U.S. calibration sphere, LCS-4 (PEAK 6G). The sphere LCS-4 is too small (1.13 m diameter) and in too high an orbit to have a sufficient SNR per pulse at VHF to be useful for this study.

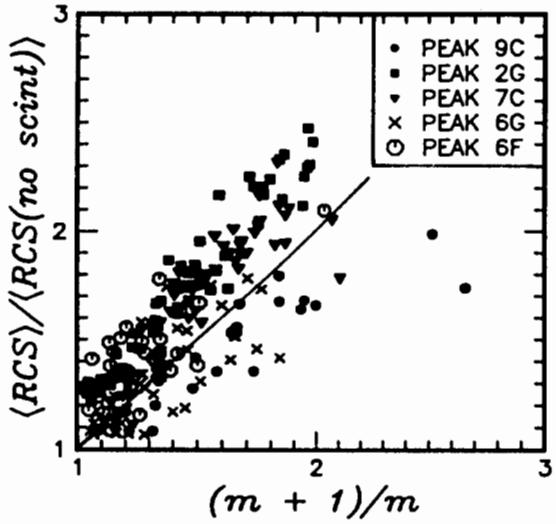

Figure 7. Comparison of ALTAIR UHF measurements to theory.

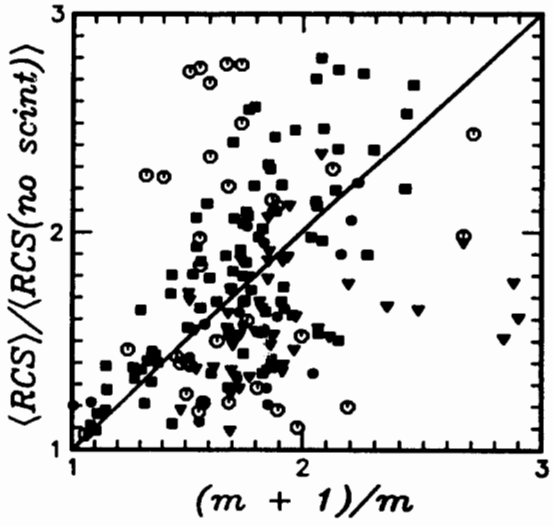

Figure 8. Comparison of ALTAIR VHF measurements to theory.

There is general agreement between the data collected in Figures 7 and 8 and the theory. The UHF data shows quite good agreement with the theory; the VHF data exhibits much more erratic behavior, most likely due to dispersive pulse spreading that causes loss in peak power not accounted for in the scattering theory, and possibly due to the reduced SNR available at VHF.

CONCLUSIONS

This paper has presented ALTAIR data illustrating the effects of severe ionospheric multipath on the received VHF wideband chirp waveform. The theory of a previously undiscovered backscatter enhancement due to scintillation is presented with convincing data as partial proof.

ACKNOWLEDGEMENT

The authors are indebted to Dr. Robert Stagat of Mission Research Corporation, Mr. Warren Dickinson of the U.S. Army Strategic Defense Command, and Dr. Leon Wittwer of the Defense Nuclear Agency for useful discussions regarding this work. The work was supported under DNA Contract No. DNA001-87-C-0169 and NRL Contract No. N00014-87-C-2336.

REFERENCES

Basu, S. E. MacKenzie, S. Basu, E. Costa, P. F. Fougere, H. C. Carlson and H. E. Whitney, "250 MHz/GHz Scintillation Parameters in the Equatorial, Polar and Auroral Environments," *IEEE Journal on Selected Areas in Communications*, Vol. SAC-5, No. 2, 1987.

Fante, R. L., "Wave Propagation in Random Media: A Systems Approach," in *Progress in Optics XXII*, E. Wolf, Ed., Elsevier, 1985.

Franke, S. J., C. H. Liu and D. J. Fang, "Multifrequency Study of Ionospheric Scintillation at Ascension Island," *Radio Science*, Vol. 19, pp. 695-706, May-June 1984.

Knepp, D. L. and J. T. Reinking, "Ionospheric Environment and Effects on Space-based Radar Detection," in *Space-Based Radar Handbook*, L. J. Cantanflo, Ed., Artech House, 1989.

Knepp, D. L., "Aperture Antenna Effects After Propagation Through Strongly Disturbed Random Media," *IEEE Trans. Antennas and Propagation*, Vol. AP-33, No. 10, pp. 1074-1084, October 1985.

Knepp, D. L., "Analytic Solution for the Two-Frequency Mutual Coherence Function for Spherical Wave Propagation," *Radio Science*, Vol. 18, No. 4, pp. 535-549, July-August 1983.

Kumagai, H., "Spatial correlations in intense ionospheric scintillations: Comparison between numerical computation and observation," *Radio Science*, Vol. 22, No. 3, pp. 439-448, May-June 1987.

Lawrence, R. S., C. G. Little and H. J. A. Chivers, "A Survey of Ionospheric Effects Upon Earth-Space Radio Propagation," *Proceedings of the IEEE*, pp. 4-27, January 1964.

Towle, D. M., "VHF and UHF Radar Observations of Equatorial *F* Region Ionospheric Irregularities and Background Densities," *Radio Science*, Vol. 15, No. 1, pp. 71-86, January-February 1980.